7048 *Inorg. Chem.* **2009**, *48*, 7048–7058
DOI: 10.1021/ic801308u

Inorganic Chemistry
Article

In Situ Phase Separation Following Dehydration in Bimetallic Sulfates: A Variable-Temperature X-Ray Diffraction Study

Diptikanta Swain and Tayur N Guru Row*

Solid State and Structural Chemistry Unit, Indian Institute of Science, Bangalore 560012, India

Received April 21, 2008

Phase separation resulting in a single-crystal−single-crystal transition accompanied by a polycrystalline phase following the dehydration of hydrated bimetallic sulfates [$Na_2Mn_{1.167}(SO_4)_2S_{0.33}O_{1.167}\cdot 2H_2O$ and $K_4Cd_3(SO_4)_5\cdot 3H_2O$] has been investigated by in situ variable-temperature single-crystal X-ray diffraction. With two examples, we illustrate the possibility of generating structural frameworks following dehydration in bimetallic sulfates, which refer to the possible precursor phases at that temperature leading to the mineral formation. The room-temperature structure of $Na_2Mn_{1.167}(SO_4)_2S_{0.33}O_{1.167}\cdot 2H_2O$ is trigonal, space group $R\bar{3}$. On heating the crystal in situ on the diffractometer, the diffraction images display spherical spots and concentric rings suggesting phase separation, with the spherical spots getting indexed in a monoclinic space group, $C2/c$. The structure determination based on this data suggests the formation of $Na_2Mn(SO_4)_2$. However, the diffraction images from concentric rings could not be indexed. In the second example, the room-temperature structure is determined to be $K_4Cd_3(SO_4)_5\cdot 3H_2O$, crystallizing in a monoclinic space group, $P2_1/n$. On heating the crystal in situ, the diffraction images collected also have both spherical spots and diffuse rings. The spherical spots could be indexed to a cubic crystal system, space group $P2_13$, and the structure is $K_2Cd_2(SO_4)_3$. The possible mechanism for the phase transition in the dehydration regime resulting in this remarkable single-crystal to single-crystal transition with the appearance of a surrogate polycrystalline phase is proposed.

Introduction

The ubiquitous role of water in the formation of hydrates of complex inorganic materials, in particular minerals, is well-recognized but little understood. Phase separation in the context of magnetic, electric, and elastic properties by individual components has been extensively studied in complex inorganic materials.[1−6] It is well-recognized that the variability in the levels of hydration results in intricate structural frameworks with hydrogen-bonded water molecules providing linkers between octahedral and tetrahedral units in mineral samples.[7−9] Further bimetallic sulfates, for example, Langbeinites, with a general formula $A_2B_2(SO_4)_3$ (where A = Li^+, Na^+, K^+, Rb^+, Cs^+, NH_4^+, etc. and B = Mn^{2+}, Fe^{2+} Co^{2+}, Ni^{2+}, Cu^{2+}, Zn^{2+}, Cd^{2+}, etc.), show interesting ferroelectric properties and phase transitions at low temperatures.[10] Compounds like Tutton's salt,[7] Leonites,[8] and Kröhnkite[9] have a general formula $A_2B(SO_4)_2\cdot XH_2O$ (where A = Li^+, Na^+, K^+, Rb^+, Cs^+, NH_4^+, etc. and B = Mn^{2+}, Fe^{2+}, Co^{2+}, Ni^{2+}, Cu^{2+}, Zn^{2+}, Cd^{2+}, etc.) with the water content (X) being six in Tutton's salt, four in Leonites, and two in Kröhnkite. It is appropriate to suggest that the temperature, pressure, and amount of hydration (sometimes even fractional) generate phases required for mineral formation, providing pointers to the origin of minerals in the earth's crust. We have observed for the first time, via in situ variable-temperature single-crystal X-ray diffraction, phase separation resulting in a single-crystal−single-crystal transition accompanied by a polycrystalline phase following dehydration in hydrated bimetallic sulfates. With two examples, we point to the possibility of producing structural frameworks following dehydration in bimetallic sulfates, which refer to the possible precursor phases at that temperature, leading to mineral formation.

*To whom correspondence should be addressed. Tel.: +91-80-22932796. Fax: +91-80-23601310. E-mail: ssctng@sscu.iisc.ernet.in.

(1) Tokura, Y. *Colossal Magmetoresistance Oxides*; Gordon and Breach: London, 1999.
(2) Dagotto, E.; Hotta, T.; Moreo, A. *Phys. Rep.* **2001**, *344*(1), 1–153.
(3) Dagotto, E. *Nanoscale Phase Separation and Colossal Magnetoresistance*; Springer: Berlin, 2002.
(4) Uehare, M.; Mori, S.; Chen, C. H.; Cheong, S. W. *Nature* **1999**, *399*, 560–563.
(5) Mori, S.; Chen, C. H.; Cheong, S. W. *Phys. Rev. Lett.* **1998**, *81*, 3972–3975.
(6) Mallison, P. M.; Rosseinsky, M. J.; Ibberson, R. M.; Price, T.; Iddles, D. M. *Appl. Phys. Lett.* **2007**, *91*, 142906.
(7) Ballirano, P.; Belardi, G. *Acta Crystallogr.* **2007**, *E63*, i56–i58.
(8) Hertweck, B.; Giester, G.; Libowitzky, E. *Am. Mineral.* **2001**, *86*, 1282–1292.
(9) Hawthorne, F. C.; Ferguson, R. B. *Acta Crystallogr.* **1975**, *B31*, 1753–1755.
(10) Nalini, G.; Guru Row, T. N. *Chem. Mater.* **2002**, *14*(11), 4729–4735.

Published on Web 07/08/2009

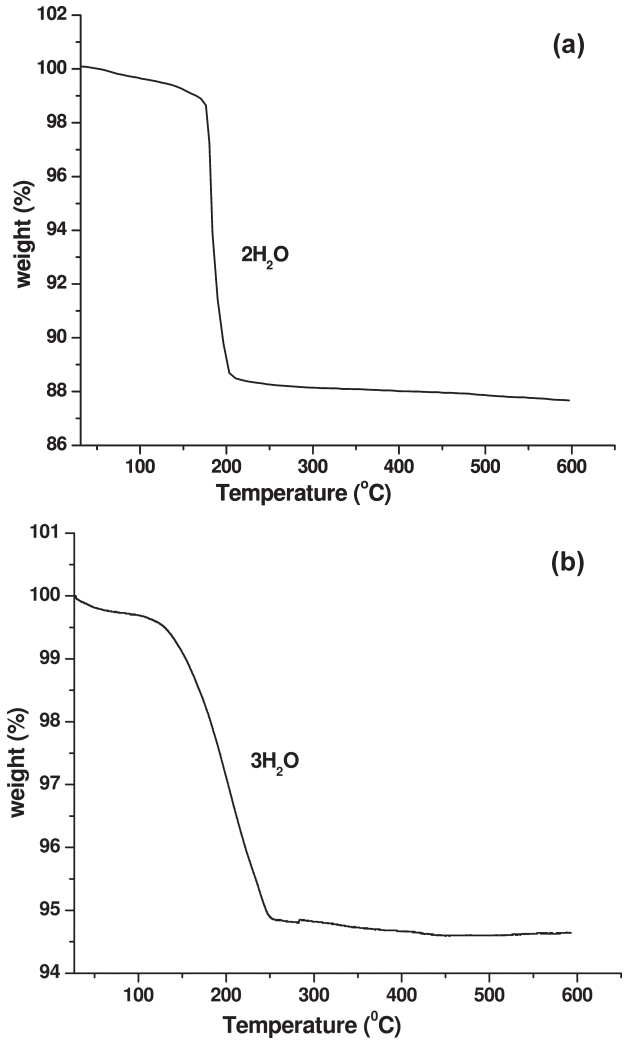

Figure 1. (a) TGA trace of $Na_2Mn_{1.167}(SO_4)_2S_{0.33}O_{1.167}\cdot 2H_2O$ indicating a stable phase after dehydration. (b) TGA trace of $K_4Cd_3(SO_4)_5\cdot 3H_2O$ indicating a stable phase after dehydration.

Experimental Section

Single crystals of both the compounds were prepared using a slow evaporation method from an aqueous solution containing equimolar quantities of Na_2SO_4 and $MnSO_4$ for $Na_2Mn_{1.167}(SO_4)_2S_{0.33}O_{1.167}\cdot 2H_2O$ and K_2SO_4 and $3CdSO_4\cdot 8H_2O$ for $K_4Cd_3(SO_4)_5\cdot 3H_2O$ at 353 K and characterized using single-crystal X-ray diffraction techniques. The quality of crystals was checked on a polarizing optical microscope in the reflection mode since the crystals were not transparent. For variable-temperature experiments, the crystal was mounted in a Lindemann glass capillary of diameter 0.5 mm, and the same crystal was used for both room- and high-temperature data acquisition. In fact, $Na_2Mn_{1.167}(SO_4)_2S_{0.33}O_{1.167}\cdot 2H_2O$ resulted during an attempt to synthesize $Na_2Mn(SO_4)_2$, which is isostructural with the $Na_2Cd(SO_4)_2$ reported earlier by us.[11] Indeed, this was an attempt to synthesize isostructural compounds to $Na_2Cd(SO_4)_2$, which are expected to find applications as fast ion conducting materials. Similar attempts to synthesize $K_2Cd(SO_4)_2$ resulted in the structure $K_4Cd_3(SO_4)_5\cdot 3H_2O$. Since both the compounds exhibited a sharp and clear loss of water molecules [two water molecules in the case of $Na_2Mn_{1.167}(SO_4)_2S_{0.33}O_{1.167}\cdot 2H_2O$ and three water molecule in the case of $K_4Cd_3(SO_4)_5\cdot 3H_2O$] in the thermogravimetric analysis (TGA) and remained without complete decomposition beyond 500 °C (Figure 1a,b), it was planned to study the structural features before and after the removal of water molecules via in situ X-ray diffraction. The diffraction data were collected on a Bruker AXS SMART APEX CCD diffractometer. The X-ray generator was operated at 50 kV and 40 mA using Mo Kα radiation. For all of the measurements, 606 frames per set were collected using SMART[12] with four different settings of φ (0°, 90°, 180°, and 270°) with the ω-scan at −0.3 scan intervals, with a counting time of 15s, while keeping the sample-to-detector

Table 1. Crystallographic Data for $Na_2Mn_{1.167}(SO_4)_2S_{0.33}O_{1.167}\cdot 2H_2O$ at 293 K and $Na_2Mn(SO_4)_2$ at 500 K

	$Na_2Mn_{1.167}(SO_4)_2S_{0.33}O_{1.167}\cdot 2H_2O$	$Na_2Mn(SO_4)_2$
temp	293K	500K
chemical formula	$Na_2Mn_{1.167}(SO_4)_2S_{0.33}O_{1.167}\cdot 2H_2O$	$Na_2Mn(SO_4)_2$
fw (M_r)	367.58	293.06
a (Å)	19.057(2)	10.101(3)
b (Å)	19.057(2)	8.240(3)
c (Å)	13.470(3)	8.730(3)
β (deg)	90.0	114.64(1)
cryst syst	trigonal	monoclinic
space group	$R\bar{3}$	$C2/c$
volume (Å^3)	4236.6(10)	660.5(4)
Z	18	4
density (g cm^{-3})	2.593	2.947
radiation type	X-ray Mo Kα	X-ray Mo Kα
cryst form, color	block, colorless	block, colorless
cryst size (mm)	0.50 × 0.30 × 0.20	0.50×0.30×0.20
diffractometer	Bruker SMART CCD area detector	Bruker SMART CCD area detector
data collection method	θ and φ scans	θ and φ scans
abs correction	SADABS	SADABS
T_{min}, T_{max}	0.5481, 0.6586	0.4036, 0.6072
no. of measured, independent, and obsd reflns	15289 2287 2082	3377 760 736
criterion for obsd reflns	$I > 2\sigma(I)$	$I > 2\sigma(I)$
R_{int}	0.049	0.0201
$\theta_{min,max}$	1.95, 28.44	3.32, 28.74
$h_{min,max}$	−25, +25	−13, +13
$k_{min,max}$	−24, +24	−11, +10
$l_{min,max}$	−17, +17	−11, +11
refinement on	F^2	F^2
$R[F^2 > 2\sigma(F^2)]$, $wR(F^2)$	0.055, 0.155	0.0961, 0.3032
GOF (S)	1.105	1.602
no. of reflns	2287	760
no. of params	168	61
H-atom treatment	fixed from geometry	no hydrogen refinement
weighting scheme	$w = 1/[\sigma^2(F_o^2) + (0.1834P)^2 + 18.3702P]$, where $P = (F_o^2 + 2F_c^2)/3$	$w = 1/[\sigma^2(F_o^2) + (0.1834P)^2 + 18.3702P]$, where $P = (F_o^2 + 2F_c^2)/3$
$\Delta\rho_{max}$, $\Delta\rho_{min}$ (e Å^{-3})	1.290, −3.379	2.510, −1.596

(11) Swain, D.; Guru Row, T. N. *Chem. Mater.* **2007**, *19*(3), 347–349.

(12) *SMART*; *SAINT*; *SADABAS*; *XPREP*; *SHELXTL*; Bruker AXS Inc.: Madison, WI, 1998.

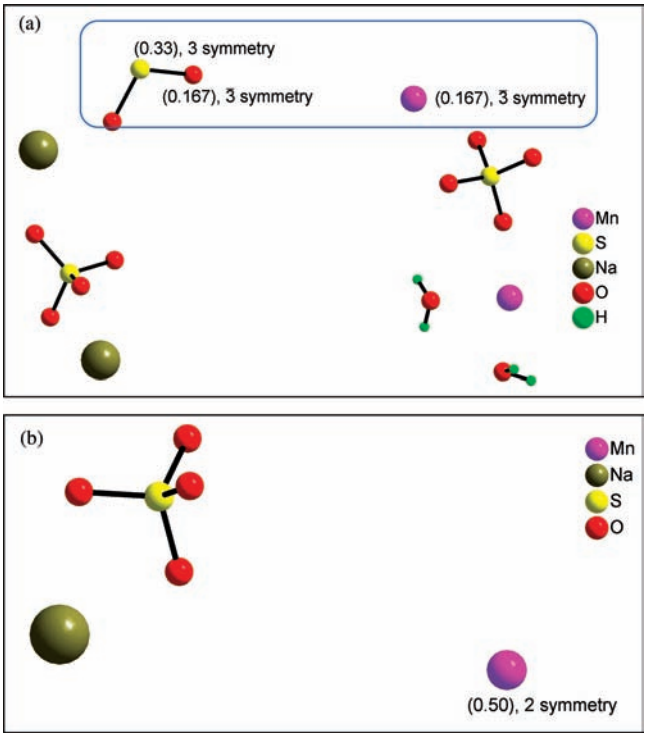

Figure 2. (a) Contents of the asymmetric unit in $Na_2Mn_{1.167}(SO_4)_2S_{0.33}O_{1.167}\cdot 2H_2O$. (b) Contents of the asymmetric unit in $Na_2Mn(SO_4)_2$.

distance at 6.054 cm and the 2θ value fixed at $-25°$. The data were processed using the SAINT-PLUS[12] protocol; an empirical absorption correction was applied using the package SADABS[13] followed by XPREP[12] to determine the space group. The structures were solved and refined using the SHELX-97[14] program present in the WinGX[15] suite. The conventional R factor is based on F; the weighted R factor "wR" and the goodness of fit "S" are based on F^2. The threshold expression of $F^2 > 2\sigma(F^2)$ is used only for calculating the R factor and is not relevant to the choice of reflections for refinements. In situ high-temperature measurement was carried out with an attached OXFORD cryosystem maintaining a heating rate of 30 K/h by using a temperature controller with a liquid N_2 flow. The details of the data collection at room temperature and at 500 K for both the compounds are given in Tables 1a,b and 4a,b, respectively.

Results and Discussion

Structure of $Na_2Mn_{1.167}(SO_4)_2S_{0.33}O_{1.167}\cdot 2H_2O$ and the High-Temperature Crystalline Phase $Na_2Mn(SO_4)_2$. The structure of the parent compound could be assigned only after careful X-ray diffraction experiments as $Na_2Mn_{1.167}(SO_4)_2S_{0.33}O_{1.167}\cdot 2H_2O$ (Figure 2a; Table 2a). On heating the parent compound on the diffractometer to 500 K and keeping the capillary at this temperature for 1 h, a remarkable structural phase separation occurs with one phase showing a single-crystal−single-crystal transition and the other generating a polycrystalline phase. The stiochiometry of the parent compound can be viewed as a combination of $Na_2Mn(SO_4)_2\cdot 2H_2O$ resembling the mineral Kröhnkite[7] with an additional ($Mn_{0.167}S_{0.333}O_{1.167}$) motif. The high-temperature single-crystal phase can be indexed in a monoclinic $C2/c$ space group, and the structure determination unequivocally suggests the formation of $Na_2Mn(SO_4)_2$ (Figure 2b; Table 2b), isostructural to $Na_2Cd(SO_4)_2$.[11] The packing features are depicted in Figure 3a,b, drawn using the package Diamond.[16] Table 3a,b represents relevant bond lengths with calculated bond valence sums (BVS) indicating the correctness of the structural assignment and the valence of the elements present at both temperatures. Figure 4 shows atomic arrangements in $Na_2Mn_{1.67}(SO_4)_2S_{0.33}O_{1.167}\cdot 2H_2O$ and $Na_2Mn(SO_4)_2 + MnS_2O_7$ as well as the 2×2 unit cell of MnS_2O_7 and a unit view of MnS_2O_7 down the c and a axes. It is of interest to note that the TGA trace shows a single phase formation after dehydration, and hence the surrogate polycrystalline phase must coexist with the crystalline phase. The CCD images before and after the phase transition are shown in Figure 5a,b, while the corresponding 3d-reciprocal lattice images are shown in Figure 6a,b, demonstrating the occurrence of this unique phase separation. The software RLATT available in the Bruker Package[12] has been used to generate these figures. Interestingly, RLATT also allows for a discrimination of phases in case there is more than one phase and assists in indexing either phase or both depending on the crystalline nature of the phase. Figure 6a clearly shows that all of the reflections belong to a single phase (blue spots) and the lattice parameters have been determined uniquely. However, Figure 6b has both indexable (blue) and nonindexable (red) spots, suggesting that there is a clear phase separation, the blue spots conforming to a crystal-to-crystal transition and the red spots belonging to the polycrystalline phase. It may be argued that, since the entire experiment is done on one single crystal in situ, the two phases after dehydration need to coexist. The possible mechanism of phase separation both in terms of symmetry considerations and in terms of possible reaction pathways has been proposed as follows.

The crystal → crystal reaction pathway is expected to be the following:

$$6[Na_2Mn_{1.167}(SO_4)_2S_{0.33}O_{1.167}\cdot 2H_2O] \xrightarrow{500\ K} 6[Na_2Mn(SO_4)_2] + MnS_2O_7 + 12H_2O$$

The utilization of six units of the parent compound for the reaction to occur is in agreement with the symmetry associated with the space group. The mechanism follows the symmetry-directed pathway from the rhombohedral → monoclinic symmetry with the removal of $\bar{3}$ symmetry, subsequent to the loss of the two coordinated water molecules. By analyzing the $Na_2Mn(SO_4)_2$ structure, it is observed that the Mn atom is at 2-fold symmetry (4e; Wyckoff) and coordinated to six oxygen atoms from sulfate tetrahedra at the general position (8f; Wyckoff) to

(13) Sheldrick, G. M. *SADABS*; University of Göttingen: Göttingen, Germany, 1996.
(14) Sheldrick, G. M. *SHELXL97*; University of Göttingen: Göttingen, Germany, 1997.
(15) Farrugia, L. J. *J. Appl. Crystallogr.* **1999**, *32*, 837–838.
(16) Brandenburg, K.; Berndt, M. *J. Appl. Crystallogr.* **1999**, *32*(5), 1028–1029.

Table 2. (a) Fractional Atomic Coordinates of $Na_2Mn_{1.167}(SO_4)_2S_{0.33}O_{1.167}\cdot 2H_2O$ and (b) $Na_2Mn(SO_4)_2$

(a) $Na_2Mn_{1.167}(SO_4)_2S_{0.33}O_{1.167}\cdot 2H_2O$

atom	Wyckoff position	symmetry element	*X*	*Y*	*Z*	U_{iso}	ocupancy
Mn(1)	18f	1	0.20106(4)	0.31689(4)	0.00125(5)	0.0136(2)	1
Mn(2)	3b	$\bar{3}$	0.3333	0.6667	0.1667	0.0114(3)	0.167
S(1)	18f	1	0.34395(6)	0.50672(6)	0.06647(8)	0.0115(3)	1
S(2)	18f	1	0.05904(6)	0.34109(6)	0.89008(8)	0.0120(3)	1
S(3)	6c	3	0.3333	0.6667	0.7867(3)	0.0612(10)	0.33
Na(1)	18f	1	0.89431(13)	0.24449(13)	0.74498(15)	0.0237(5)	1
Na(2)	18f	1	0.20644(14)	0.52970(14)	−0.01455(19)	0.0307(5)	1
O(1)	18f	1	0.3429(2)	0.58413(19)	0.0636(2)	0.0157(6)	1
O(2)	18f	1	0.2713(2)	0.4470(2)	0.0116(3)	0.0185(7)	1
O(2)	18f	1	0.3416(2)	0.4814(2)	0.1696(2)	0.0182(7)	1
O(4)	18f	1	0.4174(2)	0.5188(2)	0.0168(3)	0.0186(7)	1
O(5)	18f	1	0.0995(2)	0.2941(2)	0.9128(3)	0.0205(7)	1
O(6)	18f	1	−0.0287(2)	0.2865(2)	0.8955(3)	0.0261(8)	1
O(7)	18f	1	0.0776(3)	0.3719(3)	0.7884(3)	0.0299(9)	1
O(8)	18f	1	0.0842(3)	0.4076(2)	0.9592(3)	0.0305(9)	1
O(9)	18f	1	0.2506(5)	0.5873(6)	0.8251(6)	0.095(3)	1
O(10)	3a	$\bar{3}$	0.3333	0.6667	0.6667	0.072(4)	0.167
O(11W)	18f	1	0.1385(2)	0.3252(2)	0.1335(3)	0.0205(7)	1
O(12W)	18f	1	0.1404(3)	0.1833(2)	0.0296(4)	0.0388(11)	1
H(11A)	18f	1	0.1405	0.3681	0.1472	0.050	1
H(11B)	18f	1	0.0903	0.2912	0.1282	0.050	1
H(12A)	18f	1	0.1514	0.1646	−0.0188	0.050	1
H(12B)	18f	1	0.1762	0.1717	0.0346	0.050	1

(b) $Na_2Mn(SO_4)_2$

atom	Wyckoff position	symmetry element	*X*	*Y*	*Z*	U_{iso}	ccupancy
Mn(1)	4e	2	0.0000	0.07248(7)	0.2500	0.0190(9)	0.50
Na(1)	8f	1	0.8659(6)	0.5568(6)	0.0643(7)	0.0735(16)	1
S(1)	8f	1	0.8130(2)	0.7885(2)	0.3149(2)	0.0469(10)	1
O(1)	8f	1	0.8732(16)	0.9092(9)	0.4603(11)	0.081(3)	1
O(2)	8f	1	0.6520(10)	0.7639(10)	0.2517(12)	0.078(2)	1
O(3)	8f	1	0.8849(9)	0.6302(8)	0.3673(11)	0.070(2)	1
O(4)	8f	1	0.8365(10)	0.8465(15)	0.1716(10)	0.089(3)	1

form a distorted octahedron with 2 + 2 + 2 coordination and two short (= 2.197(6) Å), two medium (= 2.315(9) Å), and two long (= 2.392(12) Å) Mn−O bond distances (Figure 3b; Table 3b). Further, MnO_6 octahedra share corners with sulfate tetrahedra, generating two kinds of frameworks, one looking down the *z* axis and the other looking down the *y* axis. While looking down the *z* axis, the framework is made from $Mn_4(SO_4)_4$ units, which extend in the *ab* plane to form a two-dimensional sheet of dimensions 10.10 × 8.240 $Å^2$. On looking down the *y* axis, the structure forms two types of cavities made of $Mn_2(SO_4)_2$ of dimensions 5.894 × 3.987 $Å^2$ and 4.525 × 5.167 $Å^2$, and the sodium atoms located inside the cavities form weak seven coordination with oxygen atoms (Na−O = 2.355(11)−2.946(11) Å) from the sulfate tetrahedra. These loosely held Na atoms could become mobile and result in high ionic conductivity similar to that reported in the case of the isostructural compound, $Na_2Cd(SO_4)_2$.[11] In addition, the structure of $Na_2Mn_{1.167}(SO_4)_2S_{0.33}O_{1.167}\cdot 2H_2O$ has two Mn atoms, one at a general position (18f; Wyckoff) and the other at $\bar{3}$ symmetry (3b; Wyckoff; Figure 3a and Table 3a). Both of the Mn atoms generate MnO_6 octahedra with sulfate units in general positions. The formation of the S_2O_7 unit is with the sulfur atoms occupying the 3-fold symmetry (6c; Wyckoff). The Mn atom at the $\bar{3}$ position forms symmetric octahedra involving oxygen atoms associated with six sulfate units, whereas the other Mn atom in the general position associates with oxygen atoms of two water molecules (18f; Wyckoff position) and four oxygen atoms of the sulfate tetrahedra forming an asymmetric MnO_6 octahedra (Figure 3a). The two Na atoms are arranged such that the symmetric MnO_6 octahedra are surrounded by six Na atoms with NaO_7 coordination, and the second coordination around the symmetric MnO_6 is built of 12 NaO_6 units (18f; Wyckoff). On heating in situ, the removal of two H_2O molecules results in a decrease in coordination number of the other asymmetric Mn atom from 6 to 4. To keep the coordination number of the asymmetric Mn atom at 6, two additional oxygen atoms from sulfate units combine. Since the Mn atom at $\bar{3}$ symmetry and S_2O_7 at the 3-fold symmetry get associated with each other, the energy required for this association appears to be within the tolerance limits of the rhombohedral-to-monoclinic symmetry pathway, clearly suggesting that the surrogate polycrystalline phase is MnS_2O_7. The atomic arrangements in the unit cells of $Na_2Mn_{1.167}(SO_4)_2S_{0.33}O_{1.167}\cdot 2H_2O$ and $Na_2Mn(SO_4)_2$ are shown in Figure 4a and bring out the comparison. Also, Figure 4a is illustrative of the coexistence of the two phases, and Figure 4b shows the occurrence of the long-range features of the surrogate phase responsible for the appearance of the powder rings. The projection of MnS_2O_7 as viewed down the *a* axis and down the *c* axis, as shown in Figure 4c, clearly establishes

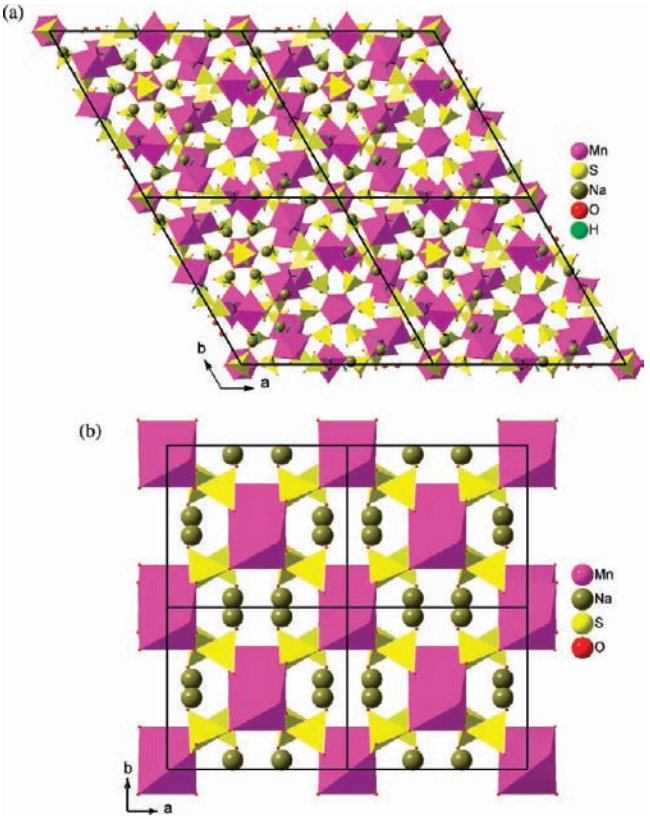

Figure 3. (a) Packing diagram prepared using DIAMOND for $Na_2Mn_{1.167}(SO_4)_2S_{0.33}O_{1.167}\cdot 2H_2O$. (b) Packing diagram prepared using DIAMOND for $Na_2Mn(SO_4)_2$.

the stoichiometry of MnS_2O_7. This observation also suggests that there is no phase segregation at the unit cell level, and as a consequence, the features are not separable in a routine high-temperature powder pattern and are not evident from the SEM/EDX analysis. It is noteworthy that the phase MnS_2O_7 has no literature reference in the ICDD database and is believed to be an unstable phase at room temperature. Since, the TGA plot (Figure 1a) indicates the stability of the mixed phase almost beyond 500 °C, it may be speculated that the two phases coexist as a composite. It must be mentioned that, as far as our knowledge goes, this is the first of its kind in the literature, and much more work needs to be done to understand the exact mechanism of this in situ X-ray study. The profile fit of the powder X-ray diffraction patterns for $Na_2Mn_{1.167}(SO_4)_2S_{0.33}O_{1.167}\cdot 2H_2O$ at 293 K and for the mixed phase $Na_2Mn(SO_4)_2 + MnS_2O_7$ at 500 K are shown in the Supporting Information (Figure S3a,b). It is also clear from the equation that every six units of $Na_2Mn(SO_4)_2$ coexist with one unit of MnS_2O_7 inside the entire single crystal as per the chemical equation:

$$[Na_2Mn_{1.167}(SO_4)_2S_{0.33}O_{1.167}\cdot 2H_2O] \xrightarrow{500\ K} 6[Na_2Mn(SO_4)_2] + MnS_2O_7 + 12H_2O$$

Structure of $K_4Cd_3(SO_4)_5\cdot 3H_2O$ and the High-Temperature Crystalline Phase $K_2Cd_2(SO_4)_3$. Attempts to crystallize $K_2Cd(SO_4)_2$, which could be isostructural to

Table 3. (a) Important Bond Distances for (a) $Na_2Mn_{1.167}(SO_4)_2S_{0.33}O_{1.167}\cdot 2H_2O$ and (b) $Na_2Mn(SO_4)_2$

(a) $Na_2Mn_{1.167}(SO_4)_2S_{0.33}O_{1.167}\cdot 2H_2O$

measure	distance (Å)	BV	measure	distance (Å)	BV
Mn1−O7	2.109(4)	0.422	Na2−O8	2.355(5)	0.255
Mn1−O5	2.126(3)	0.403	Na2−O9	2.378(9)	0.211
Mn1−O6	2.154(4)	0.374	Na2−O1	2.415(4)	0.191
Mn1−O2	2.155(3)	0.373	Na2−O2	2.465(4)	0.167
Mn1−O11W	2.193(3)	0.336	Na2−O1	2.500(4)	0.152
Mn1−O12W	2.240(4)	0.296	Na2−O3	2.640(4)	0.104
bond valence sum		2.204	Na2−O4	2.687(4)	0.092
Mn2−O1 × 6	2.173(3) × 6	0.355	bond valence sum		1.172
bond valence sum		2.130	S2−O8	1.447(4)	1.613
Na1−O8	2.313(4)	0.252	S2−O7	1.463(4)	1.545
Na1−O6	2.394(4)	0.202	S2−O6	1.464(4)	1.541
Na1−O4	2.442(4)	0.178	S2−O5	1.476(3)	1.492
Na1−O11W	2.455(4)	0.172	bond valence sum		6.191
Na1−O4	2.523(4)	0.143	S3−O10	1.616(5)	1.022
Na1−O3	2.524(4)	0.142	S3−O9 × 3	1.630(9)	0.984
bond valence sum		1.089	bond valence sum		3.974
S1−O4	1.462(3)	1.549			
S1−O3	1.464(3)	1.541			
S1−O2	1.478(3)	1.484			
S1−O1	1.486(3)	1.452			
bond valence sum		6.026			

(b) $Na_2Mn(SO_4)_2$

measure	distance (Å)	BV	measure	distance (Å)	BV
Mn1−O2	2.197(6)	0.333	Na1−O4	2.355(11)	0.225
Mn1−O2	2.197(6)	0.333	Na1−O3	2.375(9)	0.213
Mn1−O1	2.315(9)	0.242	Na1−O3	2.409(10)	0.194
Mn1−O1	2.315(9)	0.242	Na1−O4	2.626(11)	0.108
Mn1−O4	2.392(12)	0.197	Na1−O1	2.632(14)	0.106
Mn1−O4	2.392(12)	0.197	Na1−O3	2.642(9)	0.104
bond valence sum		1.938	Na1−O2	2.946(11)	0.046
S1−O4	1.449(10)	1.605	bond valence sum		0.996
S1−O3	1.470(9)	1.516			
S1−O2	1.497(8)	1.410			
S1−O1	1.526(8)	1.303			
bond valence sum		5.834			

$Na_2Cd(SO_4)_2$, generated diffraction data that could be indexed to belong to the space group $P2_1/n$, and on heating to 500 K and holding the capillary at this temperature for 60 min, as before, we get the CCD images (Figure 7a,b) which is indexed in a cubic $P2_13$ space group after the phase separation. The reciprocal lattice images showing the single- and two-phase coexistence as blue spots and red spots, as in the previous example, are shown in Figure 8a,b. The former pattern could be assigned to the structure $K_4Cd_3(SO_4)_5\cdot 3H_2O$ (Figure 9a; Table 4), where all of the atoms are in general positions (Wyckoff 4e); some are disordered with partial occupancies and show high thermal parameters (Table 5a). The three-dimensional structure is built from the corner- as well as edge-sharing of CdO_6 octahedra and SO_4 tetrahedra, with the K atoms located in the voids (Figure 10a). Important bond distances and BVS values are given in Table 6a. While on phase separation the resulting single-crystalline cubic phase with space group $P2_13$ has been shown to belong to the Langbeinite family $K_2Cd_2(SO_4)_3$ (Figure 9b), the other phase is expected to be the sought-after $K_2Cd(SO_4)_2$. The structure of $K_2Cd_2(SO_4)_3$ is a three-dimensional network of SO_4 tetrahedra and

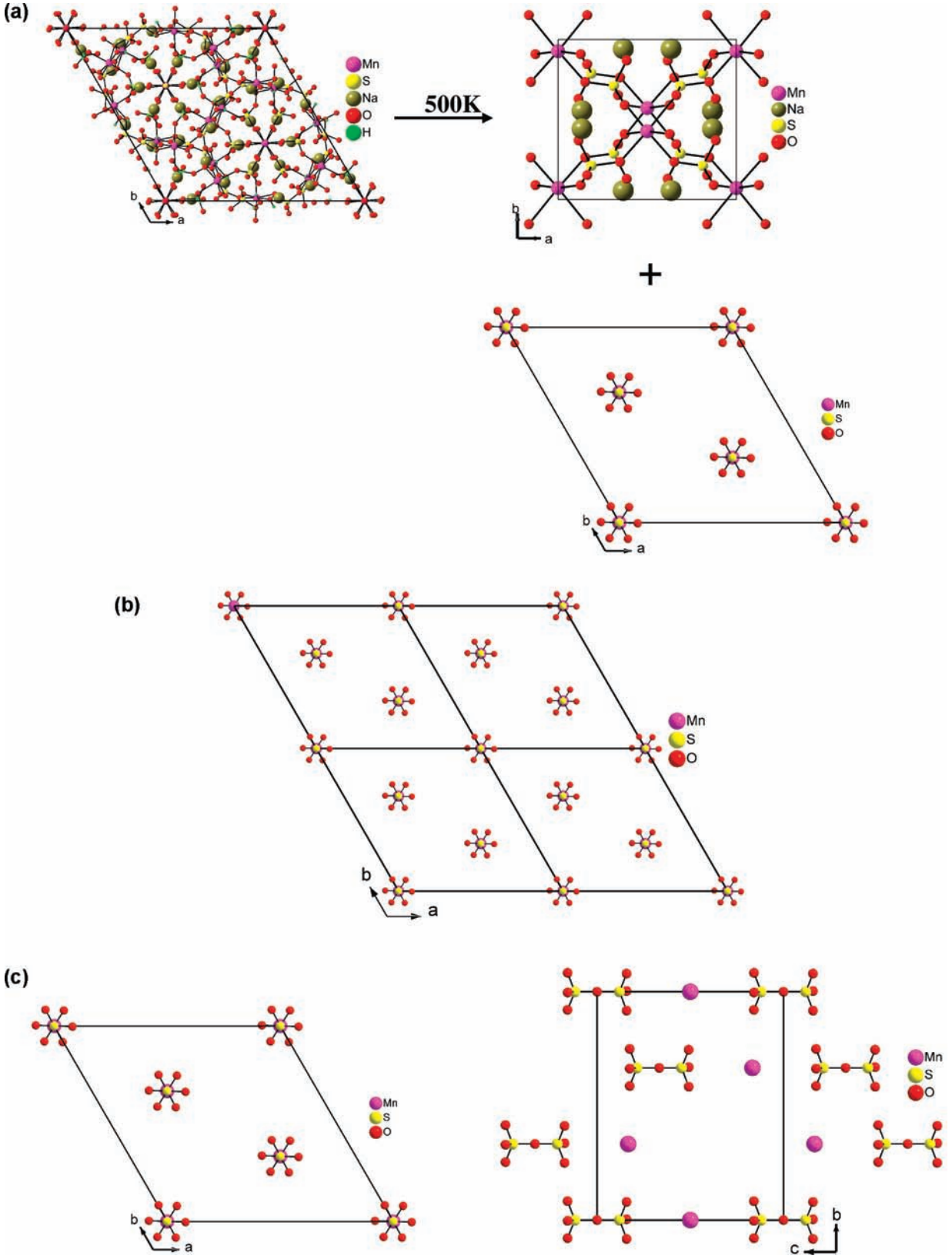

Figure 4. (a) Atomic arrangements in the $Na_2Mn_{1.167}(SO_4)_2S_{0.33}O_{1.167}\cdot 2H_2O$ phase and $Na_2Mn(SO_4)_2 + MnS_2O_7$ (after removing all other atoms from the unit cell and keeping Mn is at $\bar{3}$ symmetry and the S atom at 3-fold symmetry). (b) A 2×2 unit cell of MnS_2O_7 showing the long-range order in the arrangement, resulting in powder rings. (c) MnS_2O_7 unit view down the *c* axis and *a* axis to clarify the stoichiometry of MnS_2O_7.

CdO_6 octahedra (Figure 10b). Each tetrahedron shares its corners with four octahedra. The K and Cd atoms occupy special positions along the 3-fold axes (Wyckoff 4a), whereas the sulfur atom and oxygen atoms are in general positions (Wyckoff 12b; Table 5b). The Cd−O bond lengths in the two CdO_6 octahedra are in the range from

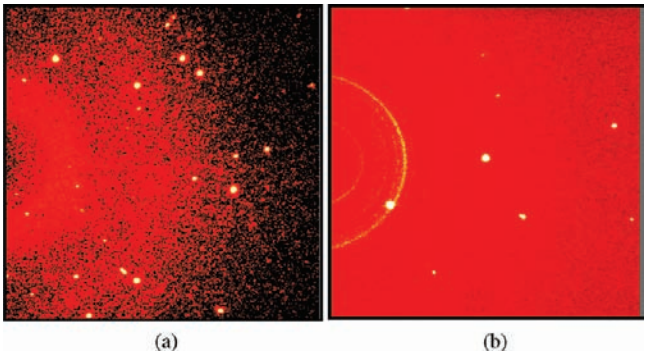

Figure 5. (a) CCD image of $Na_2Mn_{1.167}(SO_4)_2S_{0.33}O_{1.167}\cdot 2H_2O$. (b) CCD image of $Na_2Mn(SO_4)_2$.

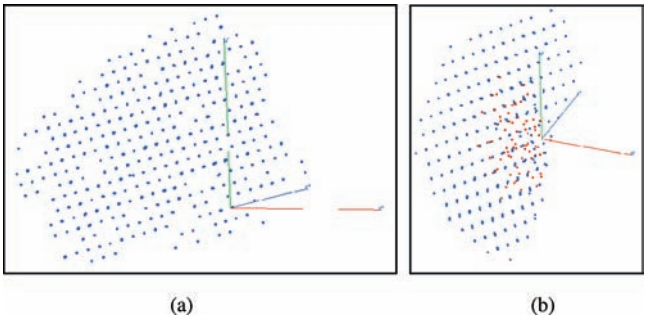

Figure 6. (a) Reciprocal lattice of $Na_2Mn_{1.167}(SO_4)_2S_{0.33}O_{1.167}\cdot 2H_2O$ [blue spots indicating single phase]. (b) Reciprocal lattice of the mixed phase of $Na_2Mn(SO_4)_2$ [blue spots] and MnS_2O_7 (?) [red spots].

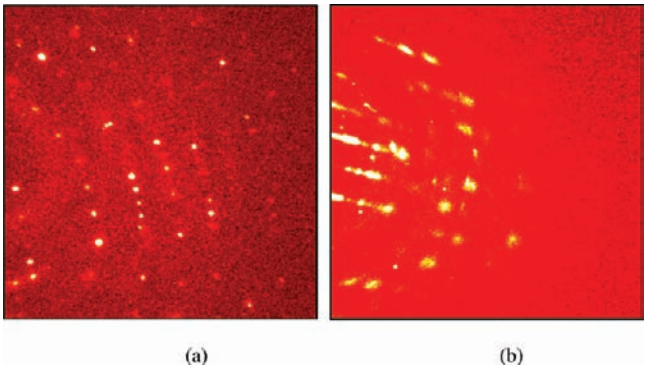

Figure 7. (a) CCD images of $K_4Cd_3(SO_4)_5\cdot 3H_2O$. (b) CCD images of $K_2Cd_2(SO_4)_3$.

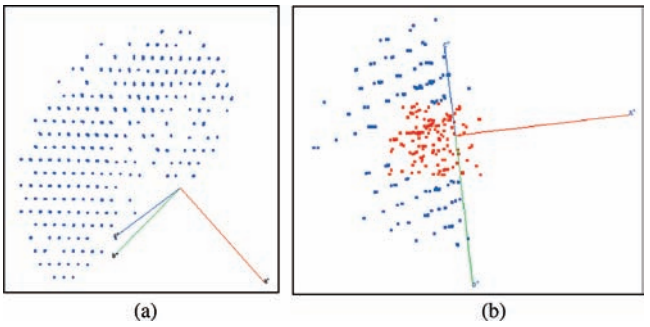

Figure 8. (a) Reciprocal lattice of $K_4Cd_3(SO_4)_5\cdot 3H_2O$ [blue spots indicating single phase]. (b) Reciprocal lattice of the mixed phase of $K_2Cd_2(SO_4)_3$ [blue spots] and $K_2Cd(SO_4)_2$ (?) [red spots].

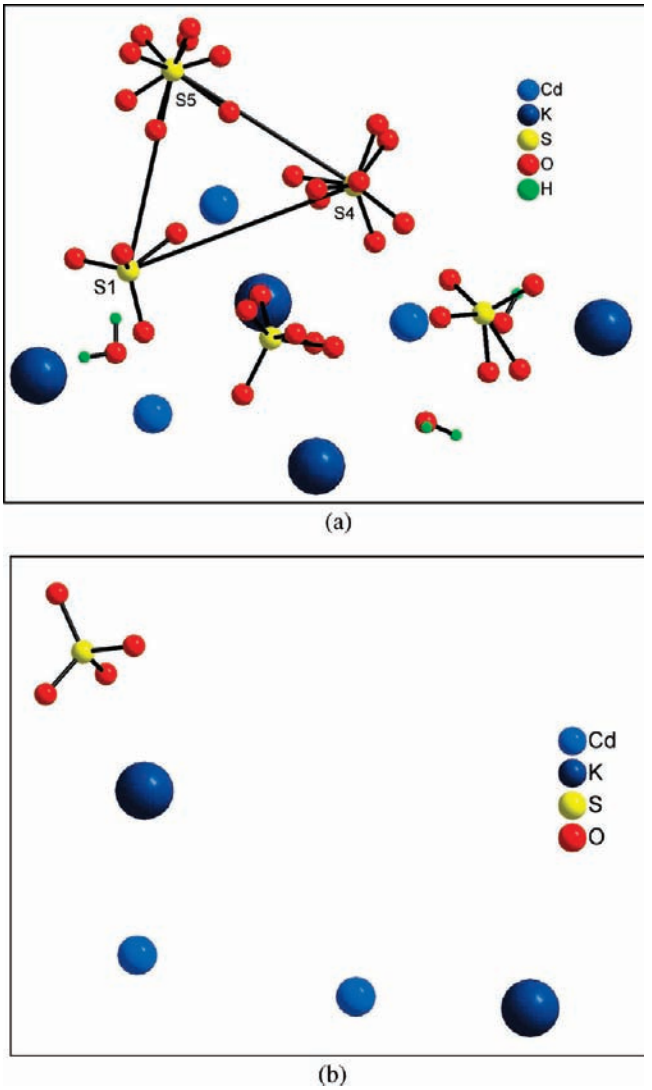

Figure 9. (a) Contents of the asymmetric unit in $K_4Cd_3(SO_4)_5\cdot 3H_2O$. (b) Contents of the asymmetric unit in $K_2Cd_2(SO_4)_3$.

2.290(2) to 2.317(15) Å and from 2.244(18) to 2.25(2) Å (Table 6b). The SO_4 tetrahedron is distorted with S−O bond distances ranging from 1.404(15) to 1.486(17) Å (Table 6b), and the O−S−O bond angles are in the range from 106.0(16) to 115.1(13)° (see the Supporting Informations, Table S2b). The potassium atoms occupy the voids of the network and are weakly coordinated to oxygen atoms, forming KO_{12} and KO_9 polyhedra. It is of interest to note that the sulfur atoms in the parent phase are almost related by a 3-fold symmetry (Figure 9a), and hence on removal of water molecules, the crystal → crystal transition is easily transformed from the monoclinic $P2_1/n$ to the cubic $P2_13$ space group with very little energy requirement. The packing diagrams shown in Figure 10a,b substantiate this observation. The atomic arrangements in the unit cell in the $K_4Cd_3(SO_4)_5\cdot 3H_2O$ phase and the $K_2Cd_2(SO_4)_3$ phase are shown in Figure 11. The cubic phase formation is hence preferred over the formation of the monoclinic phase ($C2/c$), as in the case of the previous example. Thus, the formation of the surrogate phase, which indeed could be still monoclinic ($C2/c$), gets a second preference.

Table 4. Crystal Data for $K_4Cd_3(SO_4)_5 \cdot 3H_2O$ at 293 K and $K_2Cd_2(SO_4)_3$ at 500 K

	$K_4Cd_3(SO_4)_5 \cdot 3H_2O$	$K_2Cd_2(SO_4)_3$
temp	293 K	500 K
chemical formula	$K_4Cd_3(SO_4)_5 \cdot 3H_2O$	$K_2Cd_2(SO_4)_3$
fw (M_r)	1028.03	591.18
a (Å)	9.718(1)	10.303(2)
b (Å)	16.471(2)	10.303(2)
c (Å)	14.062(2)	10.303(2)
β (deg)	109.61(2)	90.00
cryst syst	monoclinic	cubic
space group	$P2_1/n$	$P2_13$
volume (Å^3)	2120.2(4)	1093.8(4)
Z	4	4
density (g cm^{-3})	3.221	3.590
radiation type	X-ray Mo Kα	X-ray Mo Kα
cryst form, color	block, colorless	block, colorless
cryst size (mm)	0.60 × 0.50 × 0.40	0.60 × 0.50 × 0.40
diffractometer	Bruker SMART CCD area detector	Bruker SMART CCD area detector
data collection method	θ and φ scans	θ and φ scans
abs correction	SADABS	SADABS
T_{min}, T_{max}	0.0840, 0.1740	0.0533, 0.1215
no. of measured, independent, and obsd reflns	23323 5106 4703	11003 864 520
criterion for obsd reflns	$I > 2\sigma(I)$	$I > 2\sigma(I)$
R_{int}	0.0314	0.0613
$\theta_{min,max}$	1.97, 28.64	3.42, 28.39
$h_{min,max}$	−12, +12	−13, +13
$k_{min,max}$	−21, +21	−13, +13
$l_{min,max}$	−18, +18	−13, +13
refinement on	F^2	F^2
$R[F^2 > 2\sigma(F^2)]$, $wR(F^2)$	0.0740, 0.1616	0.0657, 0.1296
GOF (S)	1.068	1.016
no. of reflns	5106	864
no. of params	440	58
H-atom treatment	fixed from geometry	no hydrogen refinement
weighting scheme	$w = 1/[\sigma^2(F_o^2) + (0.1834P)^2 + 18.3702P]$, where $P = (F_o^2 + 2F_c^2)/3$	$w = 1/[\sigma^2(F_o^2) + (0.1834P)^2 + 18.3702P]$, where $P = (F_o^2 + 2F_c^2)/3$
$\Delta\rho_{max}$, $\Delta\rho_{min}$ (e Å^{-3})	3.934, −4.353	1.119, −1.114

However, it must be pointed out that the energy involvement is so subtle that a composite phase is again realized. The profile fit of the powder X-ray diffraction pattern for $K_4Cd_3(SO_4)_5 \cdot 2H_2O$ at 293 K and that for the mixed phase $K_2Cd_2(SO_4)_3 + K_2Cd(SO_4)_2$ at 500 K are shown in the Supporting Information (Figure S4a,b). Figure S4b indicates that the surrogate phase is most likely $K_2Cd(SO_4)_2$, and the deviations indicate the nature of the disorder phase. As in the previous example, it is once again difficult to derive the phases from powder diffraction and other cognate techniques including SEM/EDX, as the TGA plot in Figure 1b clearly suggests no decomposition of the coexistence of phases beyond 500 K. The crystal → crystal reaction pathway is predicted to be the following:

$$K_4Cd_3(SO_4)_5 \cdot 3H_2O \xrightarrow{500\ K} K_2Cd_2(SO_4)_3 + K_2Cd(SO_4)_2 + 3H_2O$$

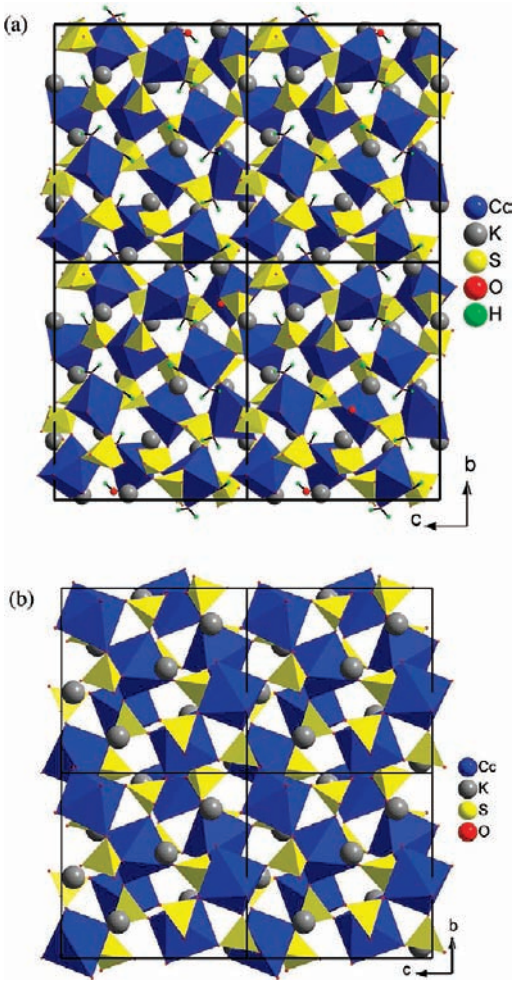

Figure 10. (a) Packing diagram prepared using DIAMOND for $K_4Cd_3(SO_4)_5 \cdot 3H_2O$. (b) Packing diagram prepared using DIAMOND for $K_2Cd_2(SO_4)_3$.

Conclusions

The study of the dehydration regime of the two compounds brings out a unique phase separation strategy based on symmetry-directed pathways and facile energy changes, keeping the lattice changes within the single-crystal to single-crystal transformation. A complete understanding of this observation needs to be explored with other precise experimental techniques and theoretical probes. However, we would like to propose a few simplistic inferences based on the above studies. Since most of the minerals occurring in nature tend to have water of hydration and the removal of water molecules from the crystal lattice in the above examples suggests phase separation upon dehydration, we believe that indeed the separated phases existed under the mineral formation conditions (temperature and pressure) in the earth's crust, and in the presence of water, a large variety of minerals got formed. The variability of the water content in different minerals thus depended on the structural nature of the precursors. Further, it is to be noted that symmetry in the precursor structural framework at the atomic level appears to govern and direct the formation of the mineral.

Table 5. Fractional Atomic Coordinates of (a) $K_4Cd_3(SO_4)_5 \cdot 3H_2O$ and (b) $K_2Cd_2(SO_4)_3$

(a) $K_4Cd_3(SO_4)_5 \cdot 3H_2O$

atom	Wyckoff position	symmetry element	*X*	*Y*	*Z*	U_{iso}	occupancy
Cd1	4e	1	0.50211(9)	0.10095(4)	0.28092(5)	0.0392(2)	1
Cd2	4e	1	0.13511(8)	0.13656(4)	0.56988(5)	0.0333(2)	1
Cd3	4e	1	0.36382(10)	0.36165(5)	0.43012(6)	0.0460(3)	1
K1	4e	1	0.2250(3)	−0.02656(15)	0.3831(2)	0.0472(6)	1
K2	4e	1	−0.2339(3)	0.25250(16)	0.50035(19)	0.0489(6)	1
K3	4e	1	0.0806(3)	0.21171(16)	0.24933(19)	0.0492(6)	1
K4	4e	1	0.8068(4)	−0.0202(2)	0.1417(2)	0.0731(10)	1
S1	4e	1	0.0656(3)	0.33247(14)	0.44948(18)	0.0367(5)	1
S2	4e	1	0.4214(3)	0.16304(15)	0.48467(17)	0.0333(5)	1
S3	4e	1	0.8562(3)	0.06870(15)	0.3717(2)	0.0389(6)	1
S4	4e	1	0.4749(3)	0.30692(14)	0.2467(2)	0.0394(6)	1
S5	4e	1	0.3422(4)	0.55999(19)	0.3861(2)	0.0513(8)	1
O1	4e	1	0.1998(12)	0.3569(5)	0.5333(7)	0.071(3)	1
O2	4e	1	0.0982(11)	0.3507(5)	0.3565(6)	0.052(2)	1
O3	4e	1	0.0387(9)	0.2456(4)	0.4559(6)	0.0455(18)	1
O4	4e	1	−0.0584(12)	0.3785(6)	0.4537(10)	0.078(3)	1
O5	4e	1	0.371(3)	0.131(2)	0.380(2)	0.073(10)	0.35
O5A	4e	1	0.5172(15)	0.131(2)	0.4443(10)	0.050(3)	0.65
O6	4e	1	0.518(2)	0.2124(11)	0.5674(11)	0.089(5)	0.75
O6A	4e	1	0.568(3)	0.154(3)	0.533(3)	0.065(13)	0.25
O7	4e	1	0.3337(9)	0.1081(4)	0.5239(7)	0.0465(18)	1
O8	4e	1	0.3344(12)	0.2228(7)	0.4123(11)	0.093(4)	1
O9	4e	1	0.9748(15)	0.0751(7)	0.3386(11)	0.094(4)	1
O10	4e	1	0.7832(18)	−0.0083(9)	0.3644(11)	0.045(3)	0.65
O10A	4e	1	0.826(2)	−0.0237(12)	0.3352(18)	0.030(5)	0.35
O11	4e	1	0.7423(13)	0.1309(7)	0.3302(9)	0.080(3)	1
O12	4e	1	0.9141(16)	0.0893(7)	0.4887(8)	0.090(4)	1
O13	4e	1	0.349(2)	0.3541(14)	0.2660(16)	0.037(4)	0.35
O13A	4e	1	0.3266(13)	0.3105(9)	0.2242(11)	0.051(3)	0.65
O14	4e	1	0.5356(17)	0.2292(8)	0.2315(17)	0.076(6)	0.60
O14A	4e	1	0.398(2)	0.2229(11)	0.2086(15)	0.047(5)	0.40
O15	4e	1	0.548(2)	0.3242(12)	0.3642(10)	0.070(6)	0.60
O15A	4e	1	0.595(2)	0.3088(13)	0.3142(19)	0.054(6)	0.40
O16	4e	1	0.5389(16)	0.3697(7)	0.1986(9)	0.045(3)	0.65
O16A	4e	1	0.4525(19)	0.3443(11)	0.1370(14)	0.028(4)	0.35
O17	4e	1	0.286(2)	0.5491(13)	0.4566(11)	0.068(5)	0.60
O17A	4e	1	0.273(2)	0.4941(13)	0.4203(18)	0.047(5)	0.40
O18	4e	1	0.431(3)	0.5495(14)	0.3490(19)	0.091(8)	0.50
O18A	4e	1	0.385(3)	0.4735(9)	0.3490(12)	0.067(6)	0.50
O19	4e	1	0.4176(18)	0.6064(11)	0.4955(14)	0.039(4)	0.40
O19A	4e	1	0.4835(15)	0.6026(7)	0.4132(9)	0.049(4)	0.60
O20	4e	1	0.2237(15)	0.6215(9)	0.3357(15)	0.043(4)	0.50
O20A	4e	1	0.257(2)	0.5888(11)	0.2803(11)	0.052(5)	0.50
O21W	4e	1	0.5378(12)	0.0455(5)	0.1419(6)	0.061(3)	1
O22W	4e	1	0.2750(9)	0.2360(5)	0.6750(6)	0.0468(18)	1
O23W	4e	1	0.4616(9)	−0.0353(4)	0.3075(6)	0.0420(17)	1
H21A	4e	1	0.4572	0.0635	0.1086	0.091	1
H21B	4e	1	0.5448	0.0734	0.0954	0.091	1
H22A	4e	1	0.2693	0.2493	0.7297	0.067	1
H22B	4e	1	0.2751	0.2795	0.6468	0.067	1
H23A	4e	1	0.4606	−0.0695	0.2648	0.059	1
H23B	4e	1	0.5348	−0.0422	0.3575	0.059	1

(b) $K_2Cd_2(SO_4)_3$

atom	Wyckoff position	symmetry element	*X*	*Y*	*Z*	U_{iso}	occupancy
Cd1	4a	3	0.83554(15)	0.83554(15)	0.83554(15)	0.0337(6)	0.33
Cd2	4a	3	0.41919(15)	1.08081(15)	0.91919(15)	0.0368(7)	0.33
K1	4a	3	0.5647(7)	1.4353(7)	0.9353(7)	0.057(3)	0.33
K2	4a	3	1.1945(6)	0.6945(6)	0.8055(6)	0.047(2)	0.33
S1	12b	1	0.5210(5)	1.7614(5)	0.8746(5)	0.0283(10)	1
O1	12b	1	0.6527(17)	1.755(2)	0.933(2)	0.081(7)	1
O2	12b	1	0.498(2)	1.895(2)	0.835(2)	0.079(6)	1
O3	12b	1	0.523(2)	1.676(2)	0.768(2)	0.096(9)	1
O4	12b	1	0.4350(19)	1.714(2)	0.9688(19)	0.082(7)	1

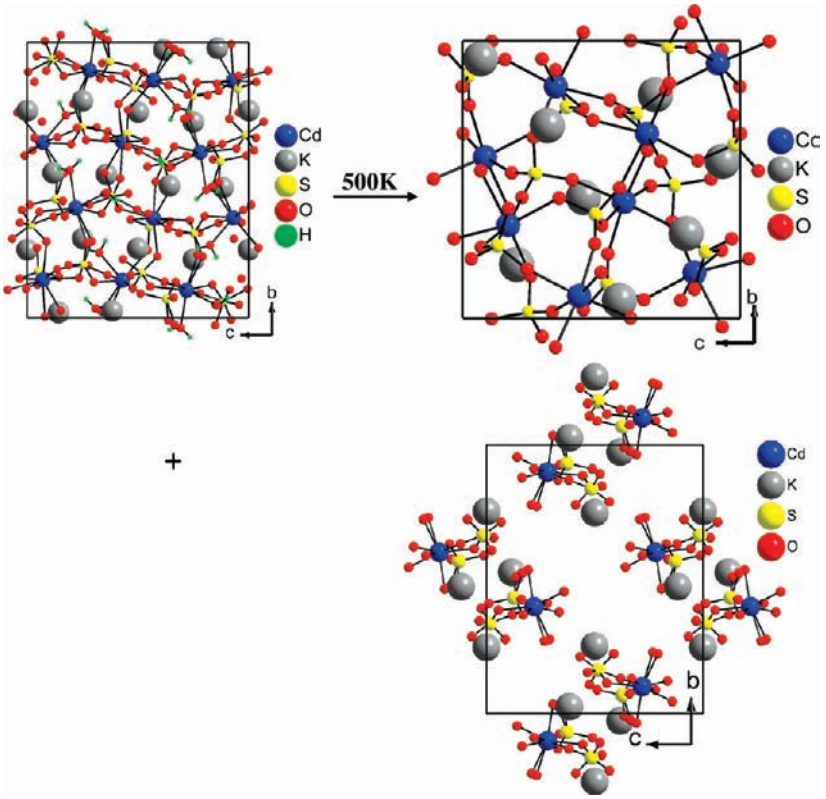

Figure 11. Atomic arrangements in $K_4Cd_3(SO_4)_5 \cdot 3H_2O$ phase and $K_2Cd_2(SO_4)_3 + K_2Cd(SO_4)_2$.

Table 6. Important Bond Distances for (a) $K_4Cd_3(SO_4)_5 \cdot 3H_2O$ and (b) $K_2Cd_2(SO_4)_3$

(a) $K_4Cd_3(SO_4)_5 \cdot 3H_2O$

measure	distance (Å)	BV	measure	distance (Å)	BV
Cd1−O5	2.240(2)	0.403 × 0.35	K1−O16A	2.693(18)	0.220 × 0.35
Cd1−O11	2.255(12)	0.387	K1−O13	2.790(2)	0.169 × 0.35
Cd1−O5A	2.263(13)	0.379 × 0.65	K1−O12	2.789(13)	0.169
Cd1−O14	2.280(12)	0.362 × 0.60	K1−O23W	2.842(9)	0.147
Cd1−O20	2.282(15)	0.360 × 0.60	K1−O9	2.844(14)	0.146
Cd1−O21W	2.288(9)	0.354	K1−O6A	2.870(4)	0.136 × 0.25
Cd1−O14A	2.324(18)	0.321 × 0.40	K1−O7	2.924(8)	0.118
Cd1−O23W	2.331(7)	0.315	K1−O5	2.970(3)	0.104 × 0.35
Cd1−O20A	2.377(19)	0.278 × 0.40	K1−O16	2.973(13)	0.103 × 0.35
bond valence sum		2.115	K1−O20A	3.030(2)	0.088 × 0.50
Cd2−O12	2.208(14)	0.440	K1−O13A	3.037(15)	0.087 × 0.65
Cd2−O10A	2.250(2)	0.393 × 0.35	K1−O18A	3.075(16)	0.078 × 0.50
Cd2−O7	2.280(8)	0.362	bond valence sum		0.963
Cd2−O16A	2.294(16)	0.349 × 0.35	K2−O15	2.615(18)	0.271 × 0.60
Cd2−O16	2.301(12)	0.342 × 0.65	K2−O6A	2.670(3)	0.234 × 0.25
Cd2−O22W	2.317(8)	0.328	K2−O16A	2.680(19)	0.227 × 0.35
Cd2−O10	2.335(15)	0.312 × 0.65	K2−O15A	2.750(2)	0.188 × 0.40
Cd2−O3	2.379(7)	0.277	K2−O14A	2.800(2)	0.164 × 0.40
bond valence sum		2.092	K2−O4	2.897(11)	0.126
Cd3−O19	2.095(16)	0.597 × 0.40	K2−O3	2.922(9)	0.118
Cd3−O18A	2.212(15)	0.435 × 0.50	K2−O6	2.940(2)	0.113 × 0.25
Cd3−O13	2.270(2)	0.372 × 0.35	K2−O19	2.943(19)	0.112 × 0.40
Cd3−O19A	2.282(11)	0.360 × 0.60	K2 -O11	3.069(12)	0.079
Cd3−O8	2.308(12)	0.336	K2−O20	3.080(2)	0.077 × 0.50
Cd3−O17A	2.340(2)	0.308 × 0.40	K2−O12	3.079(13)	0.077
Cd3−O15	2.350(2)	0.300 × 0.60	bond valence sum		0.948
Cd3−O2	2.444(10)	0.232	K3−O20A	2.686(16)	0.224 × 0.50
Cd3−O1	2.491(12)	0.205	K3−O2	2.715(8)	0.207
bond valence sum		1.928	K3−O6	2.726(16)	0.201 × 0.25
S1−O4	1.441(10)	1.640	K3−O8	2.752(12)	0.187
S1−O3	1.463(7)	1.545	K3−O19A	2.808(12)	0.161 × 0.60
S1−O2	1.476(8)	1.492	K3−O9	2.926(12)	0.117
S1−O1	1.490(9)	1.436	K3−O22W	2.927(9)	0.117

Table 6. Continued

(a) $K_4Cd_3(SO_4)_5 \cdot 3H_2O$

measure	distance (Å)	BV	measure	distance (Å)	BV
bond valence sum		6.113	K3−O20	2.963(16)	0.106 × 0.50
S2−O6A	1.360(3)	2.041 × 0.25	K3−O18	2.990(2)	0.098 × 0.50
S2−O8	1.464(11)	1.541	K3−O13A	3.009(15)	0.093 × 0.65
S2−O7	1.471(8)	1.512	K3−O5	3.100(4)	0.073 × 0.35
S2−O6	1.472(13)	1.508 × 0.75	K3−O3	3.116(8)	0.070
S2−O5A	1.478(13)	1.484 × 0.65	bond valence sum		1.145
S2−O5	1.48(2)	1.476 × 0.35	K4−O17	2.586(14)	0.293 × 0.60
bond valence sum		6.476	K4−O10A	2.660(3)	0.240 × 0.35
S3−O9	1.384(13)	1.913	K4−O18	2.750(3)	0.188 × 0.50
S3−O10	1.441(15)	1.640 × 0.65	K4−O21W	2.831(11)	0.151
S3−O11	1.477(12)	1.488	K4−O4	2.870(12)	0.136
S3−O12	1.586(11)	1.108	K4−O16	2.885(12)	0.131 × 0.65
S3−O10A	1.600(2)	1.067 × 0.35	K4−O15	2.942(17)	0.112 × 0.60
bond valence sum		5.948	K4−O18A	2.960(2)	0.107 × 0.50
S4−O15A	1.231(16)	2.893 × 0.40	K4−O15A	2.970(2)	0.104 × 0.40
S4−O13A	1.369(13)	1.992 × 0.65	K4−O19	2.980(19)	0.104 × 0.40
S4−O14	1.456(13)	1.575 × 0.60	K4−O17A	3.050(2)	0.084 × 0.40
S4−O16	1.482(12)	1.468 × 0.65	K4−O1	3.096(9)	0.074
S4−O13	1.550(2)	1.221 × 0.35	bond valence sum		1.044
S4−O14A	1.577(19)	1.135 × 0.40	S5−O18	1.160(3)	3.505 × 0.50
S4−O15	1.590(14)	1.096 × 0.60	S5−O17	1.294(17)	2.440 × 0.60
S4−O16A	1.607(18)	1.047 × 0.35	S5−O17A	1.440(2)	1.644 × 0.40
bond valence sum		6.256	S5−O19A	1.474(13)	1.500 × 0.60
			S5−O20A	1.516(14)	1.339 × 0.50
			S5−O20	1.519(13)	1.328 × 0.50
			S5−O18A	1.618(17)	1.016 × 0.50
			S5−O19	1.654(17)	0.922 × 0.40
			bond valence sum		6.983

(b) $K_2Cd_2(SO_4)_3$

measure	distance (Å)	BV	measure	distance (Å)	BV
Cd1−O1	2.290(2)	0.352	K1−O2	2.890(2)	0.129
Cd1−O1	2.290(2)	0.352	K1−O2	2.890(2)	0.129
Cd1−O1	2.290(2)	0.352	K1−O2	2.890(2)	0.129
Cd1−O4	2.317(15)	0.328	K1−O3	3.050(3)	0.084
Cd1−O4	2.317(15)	0.328	K1−O3	3.050(3)	0.084
Cd1−O4	2.317(15)	0.328	K1−O3	3.050(3)	0.084
bond valence sum		2.040	K1−O4	3.180(2)	0.059
Cd2−O3	2.244(18)	0.399	K1−O4	3.180(2)	0.059
Cd2−O3	2.244(18)	0.399	K1−O4	3.180(2)	0.059
Cd2−O3	2.244(18)	0.399	K1−O1	3.420(2)	0.031
Cd2−O2	2.250(2)	0.393	K1−O1	3.420(2)	0.031
Cd2−O2	2.250(2)	0.393	K1−O1	3.420(2)	0.031
Cd2−O2	2.250(2)	0.393	bond valence sum		0.909
bond valence sum		2.376	K2−O1	2.780(2)	0.174
S1−O4	1.404(15)	1.812	K2−O1	2.780(2)	0.174
S1−O3	1.405(18)	1.807	K2−O1	2.780(2)	0.174
S1−O2	1.460(2)	1.558	K2−O4	3.000(2)	0.096
S1−O1	1.486(17)	1.452	K2−O4	3.000(2)	0.096
bond valence sum		6.629	K2−O4	3.000(2)	0.096
			K2−O3	3.420(3)	0.031
			K2−O3	3.420(3)	0.031
			K2−O3	3.420(3)	0.031
			bond valence sum		0.903

Acknowledgment. We thank the Department of Science and Technology, India for funding and IRHPA-DST for X-ray facilities in IISc. D.S. thanks IISc for a senior research fellowship.

Supporting Information Available: Powder X-ray diffraction patterns showing the formation of the coexistence of the two phases after dehydration for both compounds (Figures S1−S4). Bond angles for all four compounds are given in Tables S1a,b and S2a,b. CIF files for all four single crystal structures reported in the article are given as well. This material is available free of charge via the Internet at http://pubs.acs.org.